Analysis on wetting and local dynamic properties of single water droplet on a polarized solid surface: A molecular dynamics study

D. Surblys,[1,a)] Y. Yamaguchi,[1,b)] K. Kuroda,[2] T. Nakajima,[2] and H. Fujimura[2]
[1]*Department of Mechanical Engineering, Osaka University, 2-1 Yamadaoka, Suita 565-0871, Japan*
[2]*Nanoscience Research Center, Dai Nippon Printing Co., Ltd., 1-1-3 Midorigahara, Tsukuba 300-2646, Japan*

(Received 22 April 2011; accepted 27 May 2011; published online 5 July 2011)

Molecular dynamics simulations of single water droplets on a solid surface were carried out in order to investigate the effects that the Coulomb interaction between liquid and solid molecules has on wetting behavior by appending vertical electric polarization on a solid surface. The water droplet became more wettable both on upward and downward polarized surfaces, although structures of the adsorption layer appearing near the solid surface were clearly different, and the relation between droplet contact angle and surface polarization was also different for upward and downward polarization directions. The probability density distribution of molecular orientation around the adsorption layer indicated that preferable water molecule orientations varied largely by the surface polarization, and the rotational mobility around the preferable orientations was also affected. The dynamic property due to this rotational mobility was clearly captured by means of distribution of rotational diffusion coefficient, which potentially corresponded to local viscosity distribution. © *2011 American Institute of Physics*. [doi:10.1063/1.3601055]

I. INTRODUCTION

Since the formulation known as Young's equation proposed in 1805, the liquid behavior on solid surfaces known as wetting has long been a topic of interest in various fields because of its considerable practical importance, and has become particularly essential in microscale processes. For instance, the required resolution for recent industrial printing has reached up to nanometer scale in the high-speed relief or gravure printing, and profound understanding of the contact behavior of a micro- or nano-scale liquid droplet on solid surface is a key issue for the control of ink motion and resulting printing quality.

Regarding molecular-scale microscopic aspect, Maruyama *et al.*[1] carried out molecular dynamics (MD) simulations of a mono-atomic van der Waals fluid on a solid surface, where the interactions between fluid and solid components were also expressed as the van der Waals type with 12-6 Lennard-Jones (L-J) form. They showed that the contact angle of the droplet had a simple first-order correlation with the potential well depth of the effective inter-atomic interaction between liquid and solid components, and they claimed that the macroscopic Young's equation could be extended to the molecular scale in this L-J system. Studies on wetting of the L-J system have also been carried out, e.g., for molecular-level surface roughness,[2] wetting of spherical particulates,[3] or sessile droplet.[4]

In the case of real fluids, however, the interactions between liquid and solid components are often also governed by the Coulomb interaction, and the above mentioned extension of Young's equation is not apparent because the Coulomb interaction has no potential well in the interaction function. Recently, wetting and adhesion structure of water molecule have also theoretically and experimentally been investigated[5–13] on specific surfaces.

In addition to the static feature of wetting expressed by the contact angle, the effect of slip at the solid-liquid interface becomes considerable in microscale liquid motion. Ligrani *et al.*[14,15] performed detailed experiments on microscale slip of water liquid, and indicated that the roughness of surface solid affected the slip length. Since the nanometer-scale roughness induced the slip difference, constraint in the motion of liquid molecules near the solid surface could be a possible cause. Considering that water is a highly polarized molecule, this constrained motion would also be provided through the Coulomb interaction with a solid surface. In any case, extracting local dynamic properties in nanometer scale should be important for further analysis on slip behavior.

In this study, we have performed MD simulations of a water droplet on a solid surface in order to investigate the effects that the Coulomb interaction between liquid and solid molecules has on wetting behavior by appending arbitrary vertical electric polarization on the solid surface. Distributions of hydrogen bond lifetime and rotational diffusion coefficient extracted as dynamic properties are also presented.

II. METHOD

A. Potential model

Water molecule is adopted as the fluid component expressed by the extended simple point charge (SPC/E, Ref. 16) potential model in this study. The 12-6 L-J and Coulomb potentials are assumed as the inter-molecular potentials between

a)Electronic mail: donatas@gcom.mech.eng.osaka-u.ac.jp.
b)Electronic mail: yamaguchi@mech.eng.osaka-u.ac.jp; http://www-gcom.mech.eng.osaka-u.ac.jp/~yamaguchi/.

the positions of the hydrogen and oxygen atoms, respectively, as in Eqs. (1) and (2):

$$\Phi^{\mathrm{LJ}}(r_{ij}) = H(r_c - r_{ij}) \cdot 4\epsilon_{ij} \left[\left(\frac{\sigma_{ij}}{r_{ij}} \right)^{12} - \left(\frac{\sigma_{ij}}{r_{ij}} \right)^{6} + \left\{ c_2^{\mathrm{LJ}} \left(\frac{r_{ij}}{r_c} \right)^2 - c_0^{\mathrm{LJ}} \right\} \right], \tag{1}$$

$$\Phi^{\mathrm{C}}(r_{ij}) = H(r_c - r_{ij}) \frac{q_i q_j}{4\pi\epsilon_0} \left[\frac{1}{r_{ij}} + \frac{1}{r_c} \left\{ c_2^{\mathrm{C}} \left(\frac{r_{ij}}{r_c} \right)^2 - c_0^{\mathrm{C}} \right\} \right], \tag{2}$$

where r_{ij} is the distance between positions of hydrogen or oxygen i and j, and ϵ_{ij}, σ_{ij}, q_i, and ϵ_0 denote the L-J energy and length parameters, point charge at site i, and dielectric constant, respectively. These interactions in Eqs. (1) and (2) are rounded off at a cut-off distance r_c using the Heaviside step function H, and a quadric function is appended so that the potential smoothly becomes zero at $r_{ij} = r_c$ with the following coefficients:

$$c_2^{\mathrm{LJ}} = 6 \left(\frac{\sigma_{ij}}{r_c} \right)^{12} - 3 \left(\frac{\sigma_{ij}}{r_c} \right)^{6}, \tag{3}$$

$$c_0^{\mathrm{LJ}} = 7 \left(\frac{\sigma_{ij}}{r_c} \right)^{12} - 4 \left(\frac{\sigma_{ij}}{r_c} \right)^{6}, \tag{4}$$

$$c_2^{\mathrm{C}} = \frac{1}{2}, \tag{5}$$

$$c_0^{\mathrm{C}} = \frac{3}{2}. \tag{6}$$

The cut-off distance r_c is set as 1.5 nm in this study. There is no L-J interaction for inter-molecular H–H and O–H in the SPC/E model.

An fcc crystal is assumed as the solid wall, and interaction between nearest neighbors is expressed by the following harmonic potential:

$$\Phi^{\mathrm{H}}(r_{ij}) = \frac{k}{2}(r_{ij} - r_0)^2, \tag{7}$$

where r_0 and k denote the equilibrium distance and the spring constant, respectively.

The interactions between fluid and solid particles are also expressed by the L-J potential and the Coulomb potential. The inter-L-J energy parameter between oxygen and wall atom $\sigma_{\mathrm{o-wall}}$ is empirically defined so that the contact angle of water droplet becomes approximately 90° in the case of no surface polarization, i.e., $q_{\mathrm{top}} = 0$ mentioned in Sec. II B.

TABLE I. Potential parameters.

$\sigma_{\mathrm{O–O}}$ (nm)	$\epsilon_{\mathrm{O–O}}$ (J)	$\sigma_{\mathrm{wall\text{-}wall}}$[a] (nm)	$\epsilon_{\mathrm{wall\text{-}wall}}$[a] (J)	$\sigma_{\mathrm{O\text{-}wall}}$ (nm)
0.3166	1.08×10^{-21}	0.35	1.44×10^{-21}	0.3333
$\epsilon_{\mathrm{O\text{-}wall}}$ (J)	q_{H} (e)	q_{O} (e)	k (N/m)	r_0 (nm)
1.247×10^{-21}	0.4238	−0.8476	46.8	0.277

[a]Used only for Lorentz-Berthelot mixing rule.

TABLE II. Mass parameters.

m_{H} (kg)	m_{O} (kg)	m_{wall} (kg)
1.674×10^{-27}	2.657×10^{-26}	3.239×10^{-25}

The potential and mass parameters are summarized in Tables I and II. The inter-L-J parameters are determined by the Lorentz-Berthelot mixing rule. Values of platinum crystal are adopted for the lattice constant and van der Waals radius of the solid here.

B. Simulation system

Figure 1 exhibits the simulation system of a water droplet on a polarized solid surface. An fcc (111) surface of a solid crystal with three layers is located on the bottom of the calculation cell with periodic boundary conditions in x and y directions with a water droplet positioned on the surface. The region size is $18.0 \times 19.2 \times 9.0$ nm^3 consisting of 4000 water molecules and 15 600 solid atoms.

The positions of solid atoms in the bottom layer are fixed and the temperature of atoms in the second layer is controlled by the Langevin method at 298.25 K with a Debye temperature of 240 K. The velocity Verlet method with modified quaternion-constraint techniques[17,18] is applied for the integration of the Newton's equation of motion with a time step Δt of 2 fs.

In order to mimic a polarized surface, an electric charge q_{top} ranging from −0.125 e to 0.125 e is appended to each solid atom in the topmost layer, and a counter charge $q_{\mathrm{mid}} = -q_{\mathrm{top}}$ is applied to each solid atom in the middle layer in this study. Since the number of atoms in each layer is the same, the total solid surface charge is zero, even though

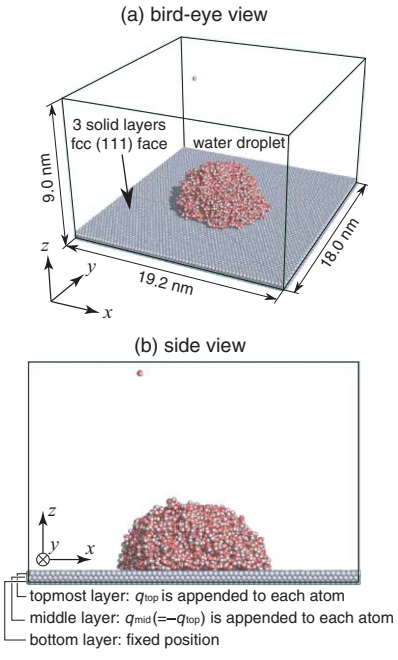

FIG. 1. Simulation system of a single water droplet on a polarized solid surface.

the surface is vertically polarized. For instance, a positive q_{top} value produces upward polarized surface. Although some parameters of platinum crystal are used here as mentioned above, the system can also be considered as a simplified model-solid with an electric dipole at the surface, due to some functional groups, for example.

All the analyses are carried out on a system equilibrated for 2 ns and distributions are obtained as the temporal average over 1 ns. We have equilibrated the system for another 2 ns for some parameters and confirmed that the statistic average did not change in these cases.[19] The equilibration time is rather short in this system since it includes a liquid-vapor interface and the droplet consists of only water molecules.

III. RESULTS AND DISCUSSION

A. Structure of a water droplet on solid surface

Figure 2 displays snapshots of the system of a water droplet on solid surfaces with different surface polarizations q_{top} and corresponding distributions of the time-averaged density and dipole moment vector in the droplet, where the axi-symmetric distribution perpendicular to the solid surface is calculated around the center of mass of the droplet. The dipole moment $u_{\text{H}_2\text{O}}$ of a single isolated water molecule is 2.35 D in the SPC/E model, and an arrow corresponding to a dipole moment of 0.4 $u_{\text{H}_2\text{O}}$ is shown below the color bar in the top-right panel. The water droplets show higher wettability with a smaller contact angle both on upward and downward polarized surfaces [Figs. 2(a-i) and 2(a-iii)] compared to that on a non-polarized surface in Fig. 2(a-ii). The contact angle is similar on the upward and downward polarized surfaces.

Regarding the density distribution, an adsorption layer with high density around 1500 kg/m^3 shown in red is observed for $q_{\text{top}} = 0$ in Fig. 2(b-ii). The second layer with above average density is also seen, and a distinct low-density region in green is observed between the first and second adsorption layers. Following a vague third layer, the density inside the droplet is almost homogeneous with a density around 1000 kg/m^3 regarded as bulk. While for $q_{\text{top}} = 0.1$ e in Fig. 2(b-iii) these density distribution features are similar, the separation between the first and second layers is not as clear for $q_{\text{top}} = -0.1$ e in Fig. 2(b-i). This indicates that the influence of surface polarization on the molecular configuration in the

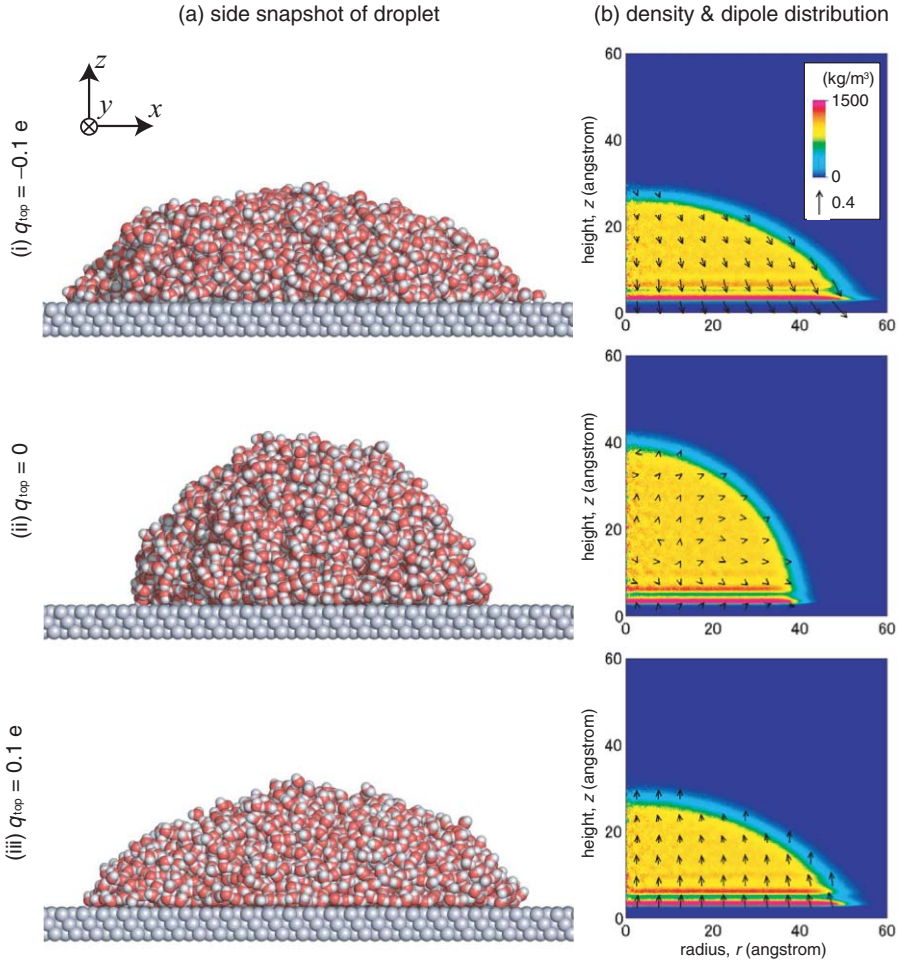

FIG. 2. (a) Side snapshots of single water droplets on solid surfaces with different surface polarization, and (b) distributions of axi-symmetric density and dipole moment around the center of mass of the droplet. The surface polarization is expressed by the electric charge on the top layer q_{top} here. An arrow corresponding to a dipole moment of 0.4 $u_{\text{H}_2\text{O}}$ is shown below the color bar in the top-right panel.

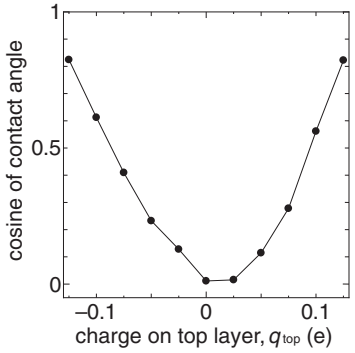

FIG. 3. Relation between contact angle of the water droplet and surface polarization expressed by the electric charge of the top layer q_{top}.

water droplet is different between upward and downward directions, although both may increase surface wettability.

In terms of dipole moment distribution, no particular direction can be seen in bulk liquid for $q_{top} = 0$ in Fig. 2(b-ii), while the vector is noticeably directed to the vapor phase at the liquid-vapor interface and slightly to the liquid phase at the solid-liquid interface. For $q_{top} = 0.1$ e in Fig. 2(b-iii), the vector configuration is basically directed upward, i.e., the oxygen atom of H_2O molecule is located beneath two hydrogen atoms. On the other hand, the configuration is essentially inversed for $q_{top} = -0.1$ e in Fig. 2(b-i) though the vector is not vertical to the surface but is slightly directed to outside, especially around the edge. On both polarized surfaces, the average dipole moment is much larger than on the non-polarized surface, and this shows that a small surface polarization would easily change the orientation of water molecules and affect the molecular configuration near the surface.

Figure 3 shows the relation between contact angle of the water droplet and surface polarization. As indicated above, both positive and negative surface polarizations would raise surface wettability, although it is hard to relate to previous research on van der Waals liquids,[1] because Coulomb potential itself does not have any potential well. This enhancement of wettability is explainable by considering that the interaction between the water molecule and the polarized surface is an integrated form of dipole-dipole interaction.[20] It should also be noted that the graph is asymmetric and the change in the contact angle is obviously different for upward and downward polarizations. This is presumably due to the difference in influence on the molecular configuration in the droplet as indicated in the difference in density distribution around the adsorption layer. We have carefully checked the contact angle with small positive q_{top} value and confirmed that the contact angle takes the maximum at $q_{top} = 0$. As dipole-dipole interaction basically gives additional adhesion force, an increase in the contact angle is not expected with surface polarization.

For further investigation on the density distribution in Fig. 2 near the solid surface, one-dimensional distributions of the number density of oxygen and hydrogen atoms are depicted in Fig. 4. The spatial average around the droplet center within $r < 20$ Å in Fig. 2 is calculated. The distributions are similar for $q_{top} = 0$ and 0.1 e in which both oxygen and hydrogen densities have the first and second peaks around $z = 3$ Å and $z = 0.6$ Å, respectively, while both peaks are sharper for $q_{top} = 0.1$ e. Considering that the intensity of the first peak of hydrogen is almost doubled against that of oxygen, it is presumable that the two hydrogen atoms in a water molecule are basically oriented parallel to the solid surface. On the other hand for the downward polarized surface with $q_{top} = -0.1$ e, the first peak of hydrogen appears closer to the surface than that of oxygen, and the intensity is smaller than that of the first peak of oxygen. This implies that one OH bond stands perpendicular to the solid surface although this configuration is not rigid.

In order to identify the molecular configuration in the vicinity of solid surface, the direction distribution of the three principal axes in molecular coordinates is analyzed and their probability density is shown in Fig. 5. The directions of the principal axes I_1 and I_2 are defined parallel to the dipole moment and the H–H line, respectively, as shown in the left panel. The direction probability density is calculated based on the angle between each principal axis and $-z$ direction,

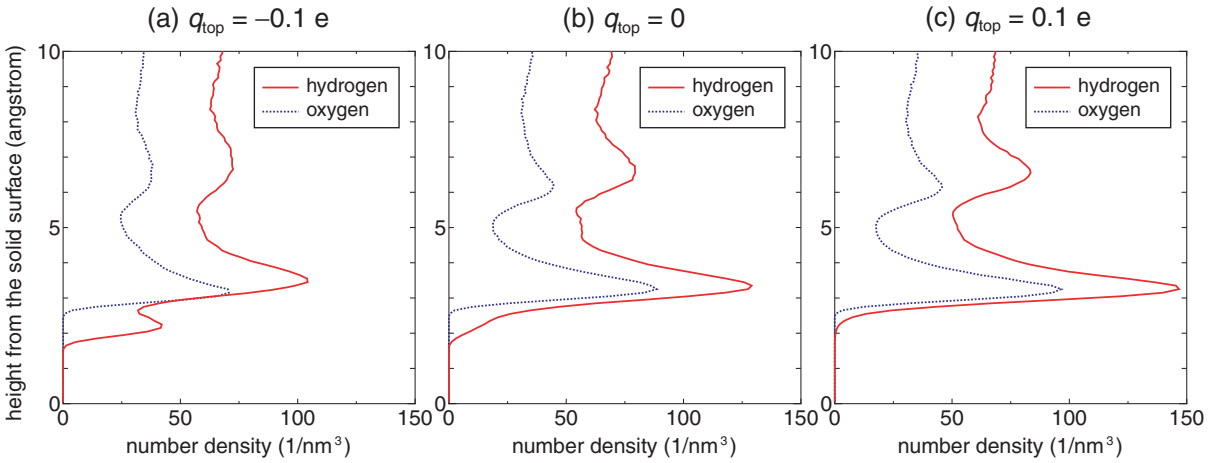

FIG. 4. One-dimensional number density distributions for hydrogen and oxygen atoms near the solid surface for different surface polarization. The distribution is obtained around the droplet center within the range of $r < 20$ Å in Fig. 2.

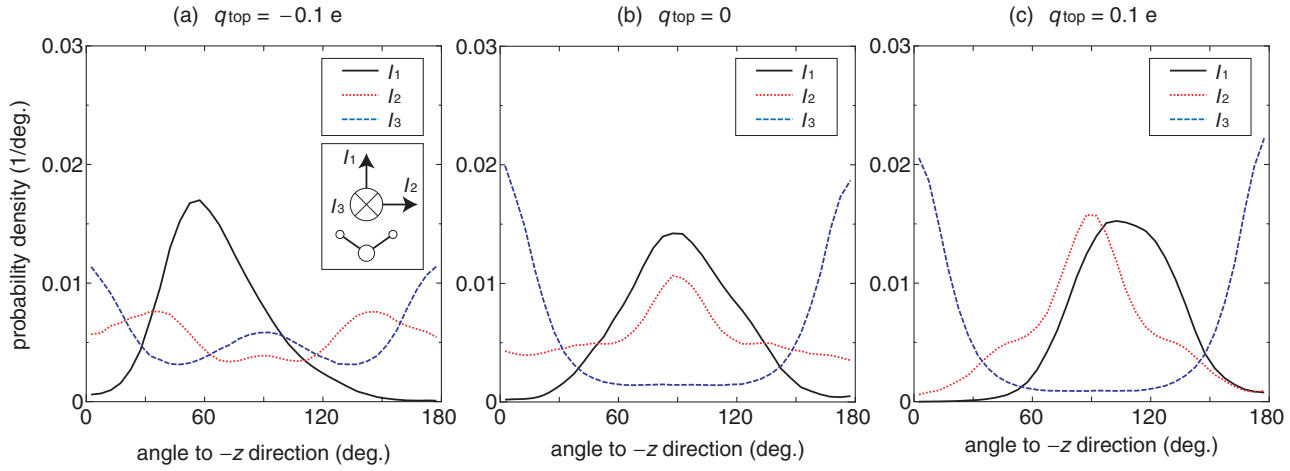

FIG. 5. Local probability density of the direction of water molecule principal axes near the solid surface for different surface polarization. The distribution is obtained around the droplet bottom-center in the height range of 3.5 Å $< z <$ 6.5 Å and radius range of $r <$ 20 Å in Fig. 2 and the angle between each principal axis and $-z$ direction is shown.

and is properly weighted considering the zenith angle. Locals in the distributions in the height range of 3.5 Å $< z <$6.5 Å and radius range of $r <$ 20 Å in Fig. 2 are shown. Regarding non-polarized surface in Fig. 5(b), both I_1 and I_2 have peaks around 90°while I_3 has two peaks around 0° and 180°. This means that the H_2O plane is basically parallel to the solid surface. It should also be noted that the peak of I_1 is rather broad, and this indicates that the water molecule fluctuates around this equilibrium orientation. On the upward polarized surface with $q_{top} = 0.1$ e in Fig. 5(c), the I_1 peak shifts to around 110° and the I_2 peak becomes sharper around 90° compared to the non-polarized surface. This implies that the rotational fluctuation is rather constrained around the equilibrium orientation with the angle between H_2O plane and surface plane around 20° while keeping the H–H line parallel to the surface. The distribution is completely different on the downward polarized surface with $q_{top} = -0.1$ e in Fig. 5(a) with each peak shifted: I_1 peak shifted to around 55°, I_2 peak divided into two smaller ones around 35°and 145°, also a small newly emerged I_3 peak is seen at 90°. As also contemplated in Fig. 4, these peak positions correspond to the equilibrium orientation with one O–H bond standing vertically to the solid surface, though the motion is not strongly constrained. It is clear from these results that the orientation of water molecules in the adsorption layer is largely affected by surface polarization, and the complex orientation induces difference in contact feature.

B. Dynamic properties in the droplet

Considering the present results, it is expected that local transport properties, such as diffusion or mobility near the solid surface, should as well be easily affected by the surface polarization inducing change in molecular orientation. In order to extract local dynamic properties, distributions of hydrogen bond lifetime and of rotational diffusion coefficient are calculated.

Figure 6 shows the distributions of the hydrogen bond lifetime for different surface polarizations, where the lifetime of inter-O–H pair within 2.5 Å and O−H···O angle over 150 is calculated. For better visualization, the value in low density region with $\rho < 300$ kg/m^3, where water molecules are considered to be out of the droplet, is depicted as zero here. Although the density and direction distributions near the surface in Figs. 2 and 5 are remarkably different, no particular distribution can be seen in the whole droplet for all surface polarizations. This means that the lifetime of hydrogen bond is not largely affected even though the molecular orientation around the adsorption layer seems completely different, and at

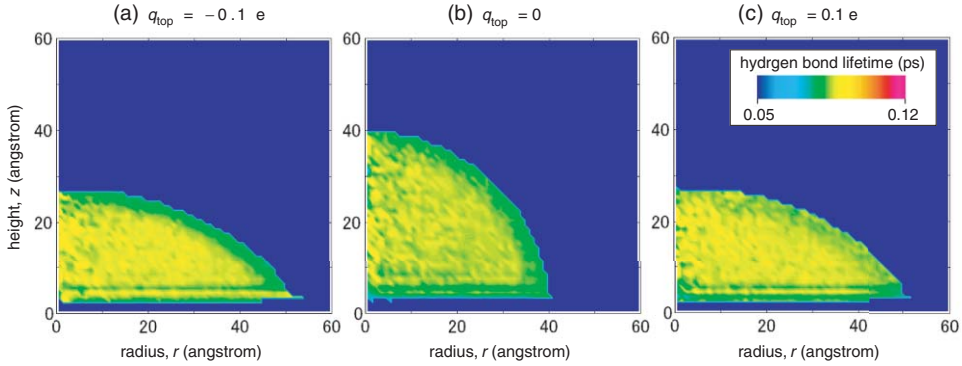

FIG. 6. Distributions of hydrogen bond lifetime in single water droplets on differently polarized solid surfaces.

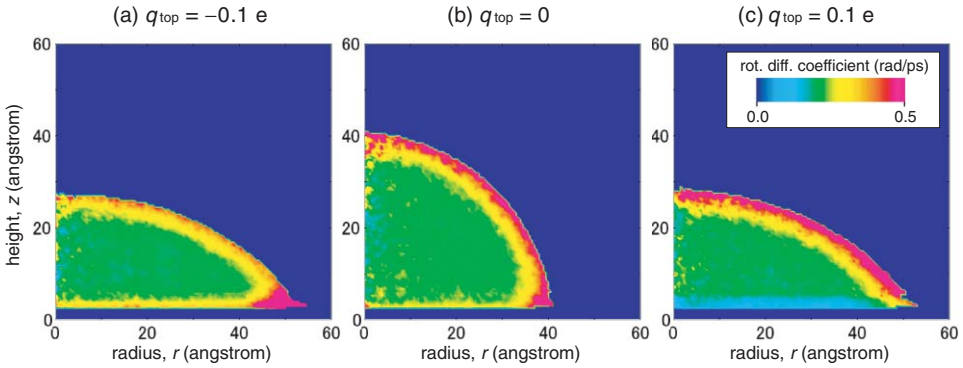

FIG. 7. Distributions of rotational diffusion coefficient in single water droplets on differently polarized solid surfaces.

least for the present case is not a good indicator of differences in dynamic properties.

Diffusion coefficient is obviously a typical indicator of the transport property. However, it is rather difficult to calculate the distribution of the local translational diffusion coefficient in a heterogeneous space, such as the nano-scale droplet in our simulation. In order to obtain translational diffusion information, the molecule has to experience enough collisions to lose ballistic behavior and to show diffusive behavior, which means that the spatial resolution of the translational diffusion coefficient is limited to the scale in which the molecule can experience enough collisions during the random motion. In order to overcome this problem, we have employed the rotational diffusion coefficient as an alternative. The rotational diffusion coefficient is originally defined as the motion of particles constrained on a spherical surface. According to the Einstein's diffusion equation,[21,22] the mean square of the angular displacement s under the Brownian motion is proportional to the elapsed time t and rotational diffusion coefficient D_{rot}, expressed as

$$\langle s^2 \rangle = 4 D_{\text{rot}} t. \tag{8}$$

Note that the dimension of the rotational diffusion coefficient D_{rot} has a dimension of "angle per time." We have extended this idea to the molecular rotation and calculated the rotational diffusion as the average of the mean square displacement of the principal axes in this study. Since light hydrogen atoms are located far from the water molecule center of mass and the inertia moment is small, the rotational motion shows diffusive behavior through the collisions to hydrogen atoms much faster than the translational motion in the same range of time, and this enables us to obtain the distribution with higher resolution in space.

Figure 7 shows the distributions of the rotational diffusion coefficient for different surface polarizations. The rotational diffusion coefficient is calculated from the angular displacement of a principal axis within 4 ps, and the average value for three principal axes is displayed. Since actual angular displacement s is bound below π, we projected the displacement to unbounded two-dimensional plane as in the Appendix. Although the diffusion coefficient in the vapor phase is actually much higher than in the droplet, the value for low density region with $\rho < 300$ kg/m^3 is depicted as zero for better visualization as in Fig. 6. For all cases, the rotational diffusion is larger at the liquid-vapor interface than in the bulk. It also becomes large around the surface for $q_{\text{top}} = 0$ and −0.1 e, where this feature is more remarkable for $q_{\text{top}} = -0.1$ e. On the other hand, the rotational diffusion coefficient around the surface is obviously lower than that in the bulk in the case of $q_{\text{top}} = 0.1$ e. As mentioned in the density distribution in Fig. 2 and direction distribution of water principal axes in Fig. 5, the rotational motion is rather constrained in the adsorption layer on the upward polarized surface with $q_{\text{top}} = 0.1$ e, while it is not strongly restricted on the downward polarized surface with $q_{\text{top}} = -0.1$ e, and these results agree well with the rotational diffusion coefficient here.

It should be noted that the translational diffusion coefficient D_{trans} is related to viscosity through the Stokes-Einstein equation:[21]

$$D_{\text{trans}} = \frac{kT}{6\pi\mu R_{\text{trans}}}, \tag{9}$$

where μ, R_{trans}, k, and T denote the viscosity, effective particle radius for translational motion, Boltzmann constant, and temperature, respectively. Similarly, the rotational diffusion coefficient D_{trans} is theoretically inversely proportional to viscosity through the Stokes-Einstein-Debye relation:[21]

$$D_{\text{rot}} = \frac{kT}{8\pi\mu R_{\text{rot}}^3}, \tag{10}$$

where R_{rot} is the effective particle radius for rotational motion. Equations (9) and (10) are originally derived for the Brownian motion of a microscale particle in a fluid; however, if the relation in Eq. (10) can be extended to the molecular rotational motion, the distribution in Fig. 7 may express the nanoscale viscosity distribution. Thus, this method to extract local distribution of the rotational diffusion coefficient can be applicable as a potential tool to obtain a nanometer-scale local fluid property. It should also be mentioned that this difference in the rotational diffusion coefficient cannot be extracted using the lifetime of hydrogen bond, which has a shorter time scale of less than 1 ps.

IV. CONCLUDING REMARKS

Molecular dynamics simulations of a single water droplet on a solid surface were carried out in order to investigate the effects that the Coulomb interaction between liquid and solid

molecules has on wetting behavior by appending surface electric polarization on a solid surface.

The water droplet became more wettable both on upward and downward polarized surfaces; however, structures of the adsorption layer appearing in the vicinity of solid surface were clearly different, and the relation between droplet contact angle and surface polarization was also different for upward and downward polarization directions. The probability density distribution of molecular orientation around the adsorption layer indicated that preferable water molecule orientations were largely varied by the surface polarization, and the rotational mobility around these preferable orientations seemed to be affected. The dynamic property due to this rotational mobility was clearly captured by means of the distribution of rotational diffusion coefficient, which potentially corresponded to local viscosity distribution.

ACKNOWLEDGMENTS

We appreciate our former group member Mr. Kazuya Ogawa for his great contribution to this work. We also thank Mr. Satoshi Nakaoka for fruitful discussion. This research is partially supported by the Ministry of Education, Science, Sports, and Culture, Grant-in-Aid for Young Scientists (B), 22760131, 2010.

APPENDIX: CALCULATION OF ROTATIONAL DIFFUSION COEFFICIENT

The angular displacement of principle axes is projected on two-dimensional plane to make reliable calculation possible. Let $\vec{e}_i$ and S_i be the unit vector of a principle axis and corresponding position on a unit sphere at ith time step as shown in Fig. 8(a), the displacement to the next time step is the length of arc $\overset{\frown}{\mathrm{S}_i\mathrm{S}_{i+1}}$. We project the point trajectory $\mathrm{S}_{i-1} \rightarrow \mathrm{S}_i \rightarrow \mathrm{S}_{i+1}$ onto a two-dimensional plane in Fig. 8(b) as $\mathrm{P}_{i-1} \rightarrow \mathrm{P}_i \rightarrow \mathrm{P}_{i+1}$ while preserving the length of the displacement equal to the arc length as well as the relative angle $\Delta\theta_i$ between $\Delta\vec{p}_{i-1,i}$ and $\Delta\vec{p}_{i,i+1}$ equal to the angle between tangential vectors of $\overset{\frown}{\mathrm{S}_{i-1}\mathrm{S}_i}$ and $\overset{\frown}{\mathrm{S}_i\mathrm{S}_{i+1}}$ at point S_i. Firstly, the length $|\Delta\vec{p}_{i,i+1}|$ from P_i to P_{i+1} is calculated as

$$|\Delta\vec{p}_{i,i+1}| = \cos^{-1}(\vec{e}_i \cdot \vec{e}_{i+1}), \tag{A1}$$

because $\vec{e}_i$ and $\vec{e}_{i+1}$ are unit vectors. Regarding the angle, we at first consider the tangential plane of the sphere at point S_i here. Let S'_{i-1} and S'_{i+1} be the vertical projections of points S_{i-1} and S_{i+1} onto the tangential plane, then $\Delta\theta_i$ is equal to the angle between $\overrightarrow{\mathrm{S}'_{i-1}\mathrm{S}_i}$ and $\overrightarrow{\mathrm{S}_i\mathrm{S}'_{i+1}}$. Considering that $\overrightarrow{\mathrm{S}_{i-1}\mathrm{S}'_{i-1}}$ is parallel to $\overrightarrow{\mathrm{OS}_i}$, $\overrightarrow{\mathrm{OS}'_{i-1}}$ is expressed by

$$\overrightarrow{\mathrm{OS}'_{i-1}} = \vec{e}_{i-1} + k\vec{e}_i. \tag{A2}$$

Since $\overrightarrow{\mathrm{S}'_{i-1}\mathrm{S}_i}$ is perpendicular to $\overrightarrow{\mathrm{OS}_i}$, the value k is simply determined by solving

$$[\vec{e}_i - (\vec{e}_{i-1} + k\vec{e}_i)] \cdot \vec{e}_i = 0. \tag{A3}$$

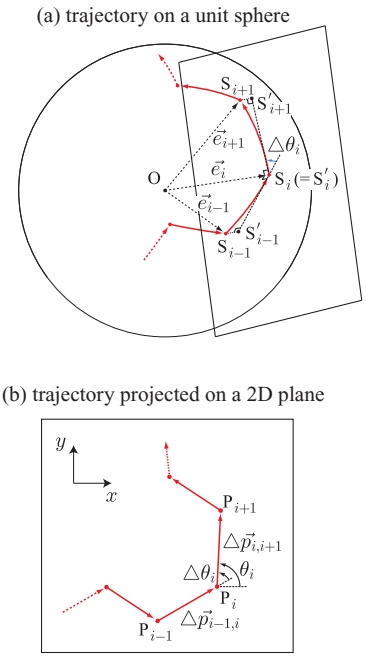

FIG. 8. Projection of angular displacement on two-dimensional plane.

Using this solution, $\overrightarrow{\mathrm{S}'_{i-1}\mathrm{S}_i}$ is expressed by

$$\overrightarrow{\mathrm{S}'_{i-1}\mathrm{S}_i} = (\vec{e}_{i-1} \cdot \vec{e}_i)\vec{e}_i - \vec{e}_{i-1}. \tag{A4}$$

Thus, the angle $\Delta\theta_i$ is determined by solving

$$\Delta\theta_i = \mathrm{sgn}\left(\vec{e}_i \cdot \left(\overrightarrow{\mathrm{S}'_{i-1}\mathrm{S}_i} \times \overrightarrow{\mathrm{S}_i\mathrm{S}'_{i+1}}\right)\right) \cdot \cos^{-1}\left(\frac{\overrightarrow{\mathrm{S}'_{i-1}\mathrm{S}_i} \cdot \overrightarrow{\mathrm{S}_i\mathrm{S}'_{i+1}}}{\left|\overrightarrow{\mathrm{S}'_{i-1}\mathrm{S}_i}\right| \left|\overrightarrow{\mathrm{S}_i\mathrm{S}'_{i+1}}\right|}\right), \tag{A5}$$

where sign function is included in order to determine the rotation direction along the radial axis $\vec{e}_i$.

Using Eqs. (A1) and (A5), the position displacement vector $\Delta\vec{p}_{i,i+1}$ in the projected plane is given by

$$\Delta\vec{p}_{i,i+1} = \left|\Delta\vec{p}_{i,i+1}\right|(\cos\theta_i,\ \sin\theta_i), \quad \theta_i = \theta_0 + \sum_{j=1}^{i}\Delta\theta_j. \tag{A6}$$

Since we are interested only in the length of relative displacement, the initial angle θ_0 is set to zero. The angular displacement $s_{0,n}$ within n steps is approximated by integrating $\vec{p}_{i,i+1}$.

$$s_{0,n} = \left|\Delta\vec{p}_{0,n}\right|, \quad \Delta\vec{p}_{0,n} = \sum_{i=0}^{n-1}\Delta\vec{p}_{i,i+1}. \tag{A7}$$

[1] S. Maruyama, T. Kuruashige, S. Matsumoto, Y. Yamaguchi, and T. Kimura, Microscale Thermophys. Eng. **2**, 49 (1998).
[2] J. Z. Tang and J. G. Harris, J. Chem. Phys. **103**, 8201 (1995).
[3] F. Bresme and N. Quirke, J. Chem. Phys. **110**, 3536 (1999).
[4] P. van Remoortere, J. E. Mertz, L. E. Scriven, and H. T. Davis, J. Chem. Phys. **110**, 2621 (1999).
[5] A. Catellani, G. Cicero, and G. Galli, J. Chem. Phys. **124**, 024707 (2006).
[6] V. C. Weiss, J. Chem. Phys. **125**, 084718 (2006).

[7]M.-C. Yeh, C.-M. Chen, and L.-J. Chen, J. Chem. Phys. **128**, 044719 (2008).
[8]G. Zimbitas, M. E. Gallagher, G. R. Darling, and A. Hodgson, J. Chem. Phys. **128**, 074701 (2008).
[9]J. D. Halverson, C. Maldarelli, A. Couzis, and J. Koplik, J. Chem. Phys. **129**, 164708 (2008).
[10]T. Schiros, O. Takahashi, K. J. Andersson, H. Öström, L. G. M. Pettersson, A. Nilsson, and H. Ogasawara, J. Chem. Phys. **132**, 094701 (2010).
[11]A. Oleksy and J.-P. Hansen, J. Chem. Phys. **132**, 204702 (2010).
[12]S. Standop, A. Redinger, M. Morgenstern, T. Michely, and C. Busse, Phys. Rev. B **82**, 161412(R) (2010).
[13]P. Varilly, A. J. Patel, and D. Chandler, J. Chem. Phys. **134**, 074109 (2011).
[14]D. Blanchard and P. Ligrani, Phys. Fluids **19**, 063602 (2007).
[15]P. Ligrani, D. Blanchard, and B. Gale, Phys. Fluids **22**, 052002 (2010).
[16]H. J. C. Berendsen, J. P. M. Postma, W. F. van Gunsteren, A. DiNola, and J. R. Haak, J. Chem. Phys. **81**, 3684 (1984).
[17]I. P. Omelyan, Comput. Phys. **12**, 97 (1998).
[18]N. S. Martys and R. D. Mountain, Phys. Rev. E **59**, 3733 (1999).
[19]W. F. van Gunsteren and A. E. Mark, J. Chem. Phys. **108**, 6109 (1998).
[20]J. N. Israelachvili, *Intermolecular and Surface Forces, Third Edition* (Academic Press, New York, 2010).
[21]R. F. Probstein, *Physicochemical Hydrodynamics* (Wiley-Interscience, New York, 1994).
[22]M. G. Mazza, N. Giovambattista, F. W. Starr, and H. E. Stanley, Phys. Rev. Lett. **96**, 057803 (2006).